

***K*-shell excitation studied for H- and He-like bismuth ions in collisions with low-*Z* target atoms**

Th. Stöhlker*

Institut für Kernphysik, University of Frankfurt, August-Euler-Straße 6, D-60486 Frankfurt and Gesellschaft für Schwerionenforschung, 64291 Darmstadt, Germany

D. C. Ionescu†

Bereich Theoretische Physik, Hahn-Meitner-Institut Berlin, Glienickerstr. 100, D-14109 Berlin, Germany

P. Rymuza

*Institut for Nuclear Studies, 05-400 Swierk, Poland*F. Bosch, H. Geissel, C. Kozhuharov, T. Ludziejewski, P. H. Mokler, and C. Scheidenberger
Gesellschaft für Schwerionenforschung, 64291 Darmstadt, Germany

Z. Stachura

Institut of Nuclear Physics, 31-342 Cracow, Poland

A. Warczak

Institute of Physics, Jagiellonian University, 30-059 Cracow, Poland

R. W. Dunford

Argonne National Laboratory, Argonne, Illinois 60439

(Received 27 May 1997)

The formation of excited projectile states via Coulomb excitation is investigated for hydrogenlike and heliumlike bismuth projectiles ($Z=83$) in relativistic ion-atom collisions. The excitation process was unambiguously identified by observing the radiative decay of the excited levels to the vacant $1s$ shell in coincidence with ions that did not undergo charge exchange in the reaction target. In particular, owing to the large fine-structure splitting of Bi, the excitation cross sections to the various L -shell sublevels are determined separately. The results are compared with detailed relativistic calculations, showing that both the relativistic character of the bound-state wave functions and the magnetic interaction are of considerable importance for the K -shell excitation process in high- Z ions such as Bi. The experimental data confirm the result of the complete relativistic calculations, namely, that the magnetic part of the Liénard-Wiechert interaction leads to a significant reduction of the K -shell excitation cross section. [S1050-2947(98)00801-4]

PACS number(s): 34.50.Fa, 34.10.+x

I. INTRODUCTION

Besides electron-capture processes Coulomb excitation is the most important production process of characteristic projectile photons in swift encounters of high- Z ions with target atoms. In contrast to the electron-capture processes, which were studied in great detail at relativistic collision conditions [1,2], no experimental data for collisionally induced projectile excitation of high- Z ions are available. In contrast, this process has been the subject of extensive experimental investigations for light and purely nonrelativistic systems such as $p \rightarrow H$, where $1s \rightarrow 2p$ transitions were studied in great detail [3–5]. Moreover, by utilizing 0° Auger spectroscopy, state selective K -shell excitation studies have also been performed, e.g., for Li-like Ne^{7+} colliding with gaseous targets

at high collision energies [6,7]. For highly charged, medium- Z ions, the experimental information about this process is rather scarce. Here, experimental investigations have been reported for ions such as H- and He-like Fe and Kr, where special emphasis was given to saturation effects for increasing nuclear charge of the target [8–11]. For high- Z ions, such studies allow one to investigate the importance of the relativistic bound-state wave functions for the dynamics in relativistic ion-atom collisions and to elucidate, in particular, the effects caused by the magnetic part of the Liénard-Wiechert interaction [12,13]. Until now, information about these effects was experimentally accessible only by the study of projectile ionization cross sections, which turned out to be rather insensitive to relativistic effects [14,15].

The formation of excited states via Coulomb excitation can be studied uniquely for one- and two-electron high- Z ions by the observation of the radiative decay of the excited levels to the ground-state. Owing to the large fine-structure splitting in such ions the cross sections for ground state excitation into the various L -shell sublevels can be unambiguously determined [16]. In particular, due to the fast

*Electronic address: t.stoehlker@gsi.de

†Present address: Lawrence Berkeley National Laboratory, 1 Cyclotron Road, Berkeley, CA 94720. Electronic address: dorin_ionescu@macmail.lbl.gov

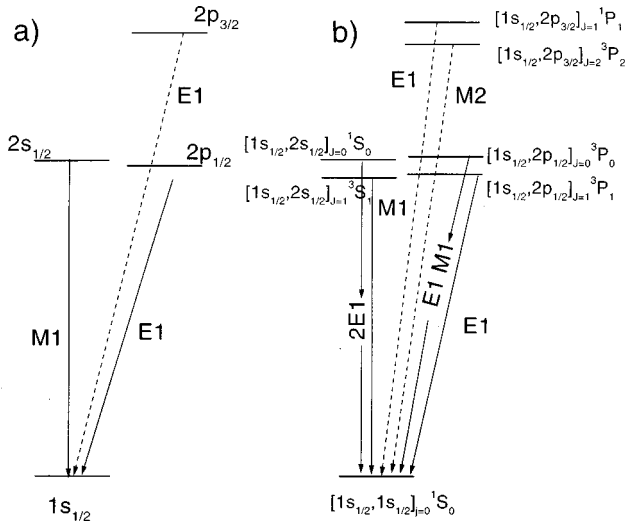


FIG. 1. Level scheme of the first excited levels in H-like and high-Z He-like ions. In addition the multiplicities of the deexcitation photons are given. The Ly- α_1 and $K\alpha_1$ transitions are depicted by the dashed arrows, whereas the Ly- α_2 and $K\alpha_2$ transitions are shown by full arrows.

$2s_{1/2} \rightarrow 1s_{1/2}$ M1 transition, excitation to the $2s_{1/2}$ level can be observed for high-Z H-like ions, whereas for low- or medium-Z systems the $2s_{1/2}$ level predominately decays via two-photon emission (2E1) [17,18]. In Fig. 1, the simplified level schemes of the first excited states in H-like ions [Fig. 1(a)] and in high-Z He-like systems [Fig. 1(b)] are depicted along with the multiplicity of the deexcitation photons. In the figure, the dashed arrows refer to the Ly- α_1 transitions in the H-like ions ($K\alpha_1$ transitions in He-like ions) whereas the full arrows mark the Ly- α_2 transitions in the one-electron systems ($K\alpha_2$ transitions in He-like ions). For the assignment of the levels in the He-like system, both the LS and the JJ coupling schemes are used in the figure. Note that within a nonrelativistic approach for Coulomb excitation in H-like systems, the $2s_{1/2}$ level can only be formed by the electric monopole part of the excitation field whereas the p levels ($2p_{1/2}$ and $2p_{3/2}$) can be populated by electric dipole excitation. Moreover, with increasing nuclear charge, the structure of the He-like ions approaches that of H-like systems (see Fig. 1), i.e., electron-electron correlation effects are small with respect to the Coulomb interaction between the electrons and the charge of the nucleus. Hence, for high-Z He-like ions the excitation cross sections should be almost unaffected by the presence of the second electron. However, it is essential to consider the correct angular-momentum coupling scheme of the two electrons. For example, monopole excitation to the L shell of He-like ions can only populate the $[1s_{1/2}, 2s_{1/2}]_{J=0,1} {}^1S_0$ level. Therefore, this does not lead to the emission of a $K\alpha$ photon, since this level can only decay by the simultaneous emission of two photons (2E1 decay).

In this paper, we report both experimental and theoretical investigations of the K -shell Coulomb excitation process for high-Z projectiles in relativistic collisions with low-Z target atoms. Our study shows that a complete relativistic description of the Coulomb interaction is required to describe the details of the excitation process in high-Z ions. In particular, the magnetic interaction becomes important only when one

considers the coherent sum of the magnetic and the electric amplitudes of the Liénard-Wiechert potential. The paper is structured as follows: In Sec. II, a relativistic treatment of the Coulomb excitation mechanism will be outlined. Thereafter, in Sec. III, the experimental method will be described. The measured x-ray spectra and the applied data analysis are discussed in Sec. IV. In Sec. V, the subshell-differential experimental and theoretical results are compared and discussed in detail. Finally, in Sec. VI, a short summary is given and possible further improvements of the experimental technique are outlined.

II. THEORY

A. H-like ions

For the calculation of transition probabilities and of cross sections for excitation of high-Z one-electron projectiles incident on light target atoms we adopt the impact parameter picture. The nuclear charge numbers of the projectile and the target are Z_P and Z_T , respectively. At relativistic velocities it is a very good approximation to assume that the projectile moves with constant velocity at an impact parameter \mathbf{b} along a classical straight-line trajectory [1]. In the following we choose the origin of the coordinate system to be the center of the heavy projectile ion. In this frame the target ion moves parallel to the z axis with constant velocity $+\mathbf{v}$, and the x - z plane is the scattering plane. The space and time coordinates of the electron in the projectile and in the target rest frame are denoted by (\mathbf{r}, t) and (\mathbf{r}', t') , respectively. In first order perturbation theory, the transition amplitude for excitation of a projectile electron may be written as [1]

$$A_{fi}(b) = i\gamma\alpha Z_T \int dt e^{i(E_f - E_i)t} \int d^3r \psi_f^\dagger(\mathbf{r}) \frac{1 - \beta \hat{\alpha}_z}{r'} \psi_i(\mathbf{r}), \quad (1)$$

where $\alpha \approx 1/137$ is the fine-structure constant, $\beta = v/c$, $\gamma = (1 - \beta^2)^{-1/2}$, and $\hat{\alpha}_z$ is the Dirac matrix in the z direction. Here and in the following we use natural units ($\hbar = m = c = 1$). Consequently, the total energies E_i and E_f of the initial and final states, respectively, are measured in units of $mc^2 \approx 511$ keV. The Lorentz transformation of the target potential from the target rest frame into the projectile rest frame yields the Liénard-Wiechert potential

$$A^\mu = \gamma \frac{\alpha Z_T}{r'} (1, 0, 0, +\beta), \quad (2)$$

where the electron-target distance, as seen in the projectile system, is denoted by $r' = \sqrt{(x-b)^2 + y^2 + \gamma^2(z-vt)^2}$.

Since for high-Z atoms or ions it is mandatory to use relativistic wave functions, we employ in the present work exact Coulomb-Dirac wave functions for the description of initial (ψ_i) and final (ψ_f) states. In the rest frame of the projectile system these are defined by eigenfunctions of the projectile Hamiltonian, i.e.,

$$\psi_{n,j,\mu}(\mathbf{r}) = \begin{pmatrix} g_\kappa(r) \chi_{\kappa\mu}(\Omega) \\ if_\kappa(r) \chi_{-\kappa\mu}(\Omega) \end{pmatrix}, \quad (3)$$

with real radial functions $g_{\kappa}(r)$ and $f_{\kappa}(r)$. The angle-dependent functions $\chi_{\kappa\mu}(\Omega)$ are spherical spinors as defined in [1,19]. The Dirac angular momentum quantum number $\kappa = \pm(j+1/2)$ is the eigenvalue of the operator $\hat{K} = \hat{\gamma}_0 (\hat{\sigma} \cdot \hat{L} + 1)$ and μ is the magnetic quantum number. Owing to the spherical symmetric projectile potential, we have to deal with a radial quantum number n , a total angular momentum quantum number j , a magnetic quantum number μ , and parity. Introducing the minimum momentum transfer $q_0 = (E_f - E_i)/v$, the integration over the time dependence in Eq. (1) is performed with the help of the relation

$$\int_{-\infty}^{\infty} dt \frac{1}{r'} e^{i(E_f - E_i)t} = \frac{2}{\gamma v} e^{iq_0 z} K_0 \left(\frac{q_0}{\gamma} \sqrt{(x-b)^2 + y^2} \right), \quad (4)$$

where K_0 denotes the modified Bessel function. With these ingredients, the cross section for the excitation of a projectile electron between any pair of specified initial and final states, i and f , respectively, is given by the expression

$$\begin{aligned} \sigma_{fi} &= 2\pi \int_0^{\infty} db b P_{fi}(b) \\ &= 8\pi v_T^2 \int_0^{\infty} db b \left| \langle f | (1 - \beta \hat{\alpha}_z) e^{iq_0 z} \right. \\ &\quad \left. \times K_0 \left(\frac{q_0}{\gamma} \sqrt{(x-b)^2 + y^2} \right) | i \rangle \right|^2, \end{aligned} \quad (5)$$

where $\nu_T^2 = \alpha Z_T/v$ is the target Sommerfeld parameter. Here we introduced the impact-parameter-dependent transition probability $P_{fi}(b) = |A_{fi}(b)|^2$. Inspection of expression (5) shows that the range of the effective interaction, contributing to excitation, is $1/q_0$ along the beam direction, i.e., parallel to the z axis, but γ/q_0 perpendicular to it. This behavior is characteristic for the Liénard-Wiechert interaction. Equation (5) along with the projectile eigenfunctions (3) (substituted for the initial and final states) constitute our starting point for the exact numerical evaluation of excitation probabilities and corresponding cross sections.

In Fig. 2 we present weighted probabilities $bP(b)/Z_T^2$ for excitation of a $1s_{1/2}(1/2)$ electron of the bismuth projectile incident on a proton at 119 MeV/u laboratory energy. Only the leading probabilities into specific final states $n, l_j(\mu_j)$ are depicted. It should be pointed out that due to the perturbative treatment of the interaction, the calculated probabilities and the cross sections [Eq. (5)] depend quadratically on the target nuclear charge. The probability associated with the transition $1s_{1/2}(1/2) \rightarrow 2p_{3/2}(3/2)$, which is very close to the dashed-dotted curve in this figure, i.e., the transition $1s_{1/2}(1/2) \rightarrow 2p_{1/2}(-1/2)$, is not drawn. We note that the main contribution to the excitation cross section stems from the transition $1s_{1/2}(1/2) \rightarrow 2s_{1/2}(1/2)$. While the maximum value of this weighted probability is located at an impact parameter of $\lambda_C \approx 386$ fm, the other curves depicted attain their maximum values at much larger impact parameters. In addition, one can see that the excitation probabilities to the higher states extend to much larger impact parameters than for the transition to the $2s_{1/2}(1/2)$ state. This behavior is related to the radial extension of the bound-state eigenfunctions.

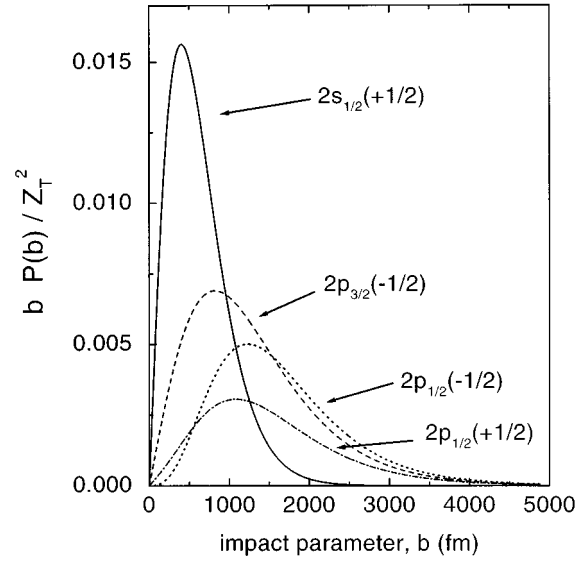


FIG. 2. Weighted excitation probabilities $P(b)b/Z_T^2$ for $\text{Bi}^{82+}[1s_{1/2}(1/2)] + Z_T$ collisions at 119 MeV/u laboratory energy as functions of the impact parameter. Only the leading probabilities into specific final states $n, l_j(\mu_j)$ are plotted.

Concerning the excitation to the $2p_{1/2}(\pm 1/2)$ states, we find that the partial cross section for the transition with $\mu_f = \mu_i - 1$ is about 50% higher than for the transition with $\mu_f = \mu_i$. A similar result was found in nonperturbative calculations of excitation cross sections based on the two-center coupled-channel formalism [20]. In order to achieve a better understanding of this behavior, we investigate the influence of the magnetic part of the Liénard-Wiechert interaction, i.e., the term proportional to the $\hat{\alpha}_z$ matrix in Eq. (5), on the partial cross sections.

In Fig. 3 we analyze the contributions associated with the different magnetic quantum numbers of the $2p_{1/2}$ state in a $\text{Bi}^{82+} + Z_T$ collision at 119 MeV/u. The ratio of the transition probability for $\mu_f = \mu_i - 1$ to the corresponding probability for $\mu_f = \mu_i$ is displayed as a function of the impact parameter. The dashed curve is obtained with the inclusion of the complete Liénard-Wiechert interaction and the solid curve is calculated by considering solely the electric part of the electron-target interaction. It is evident that the inclusion of the magnetic interaction leads to a strong increase of the relative importance of the transition with $\mu_f = \mu_i - 1$ as compared to the case with $\mu_f = \mu_i$ over the entire range of relevant impact parameters. This demonstrates that magnetic interactions of relativistic origin play an important role at the collision energies considered. One has to note that at very small impact parameters only transitions with equal magnetic quantum numbers ($\mu_f = \mu_i$) provide important contributions, since the collision system is approximately cylindrically symmetric. In particular, for central collisions ($b=0$), the multipole decomposition of the Liénard-Wiechert interaction [13] contains only angular momentum transfer with $M=0$. Since the addition rule for magnetic quantum numbers $M = \mu_f - \mu_i$ is similar to the rule encountered in nonrelativistic collisions, it follows that only transitions with $\mu_f = \mu_i$

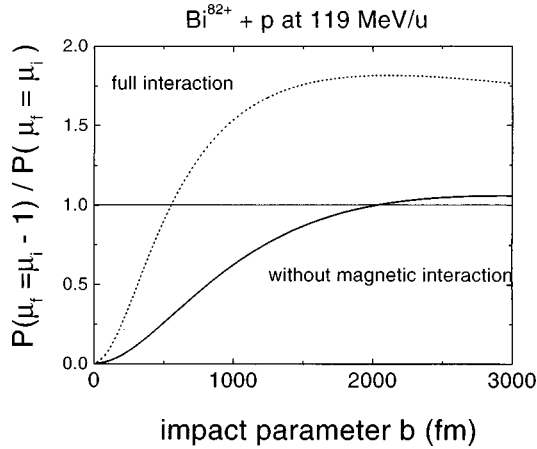


FIG. 3. The ratio of the probability for the transition $1s_{1/2}(1/2) \rightarrow 2p_{1/2}(1/2)$ ($\mu_f = \mu_i$) to the corresponding probability for the transition $1s_{1/2}(1/2) \rightarrow 2p_{1/2}(-1/2)$ ($\mu_f = \mu_i - 1$) in a $\text{Bi}^{82+} [1s_{1/2}(1/2)] + Z_T$ collision at 119 MeV/u laboratory energy as a function of the impact parameter. The dashed curve is obtained with the inclusion of the complete Liénard-Wiechert interaction and the solid curve is calculated by considering solely the electric part of the electron-target interaction.

are possible and that the displayed ratio approaches 0 for $b=0$. With increasing impact parameters, transitions with $\mu_f \neq \mu_i$ become more and more probable, since the cylindrical symmetry is broken. In fact, the calculation incorporating the complete relativistic interaction shows (Fig. 3) that for $b \geq 500$ fm the excitation probability for $\mu_f = \mu_i - 1$ is larger than for the transition with $\mu_f = \mu_i$. It should be pointed out that for relativistic velocities all angular momenta ($L=0, \dots, \infty$) of the effective interaction may contribute [12]. This behavior is distinctly different from the nonrelativistic case, where the triangle rule $|j_f - j_i| \leq L \leq |j_f + j_i|$ is strictly fulfilled.

The absolute cross-section calculations were performed for H-like Bi ions colliding with protons at energies of 82 and 119 MeV/u, by assuming that the electron is excited from the $1s$ ground state with magnetic quantum number $\mu_i = +1/2$ (see values given in the table). For the particular case of 119 MeV/u, the theoretical results obtained with the inclusion of the complete Liénard-Wiechert interaction are compared in Table I with calculations considering solely the electric part of the electron-target interaction. For the L -shell sublevels the inclusion of the magnetic part of the interaction leads to a strong *reduction* of the absolute cross-section values (17.7% for $2s_{1/2}$, 19.8% for $2p_{1/2}$, and 24.4% for $2p_{3/2}$) pointing to a destructive interference between the amplitudes for the electric and magnetic parts of the interaction. Moreover, for the particular case of excitation to the $2p_{3/2}$ state at 119 MeV/u we added the electric and magnetic amplitudes incoherently (see values in the square brackets in the table), a commonly used theoretical approach. It is interesting to note that although the interference effect is very pronounced for the case of the coherent sum, the magnetic interaction appears to be completely unimportant if the amplitudes are added incoherently. These findings underline that only a complete consideration of the Liénard-Wiechert potential allows the investigation of the role of the magnetic interaction in relativistic ion-atom collisions.

TABLE I. Total cross sections for excitation (in barn) to the L -subshell levels calculated for H-like Bi ions colliding with protons at the energy of 82 MeV/u (top part) and 119 MeV/u (bottom part), respectively. In the calculation the electron is excited from the $1s$ ground state with magnetic quantum number $\mu_i = +1/2$. The results in parentheses include solely the electric part of the electron-target interaction whereas the numbers given in square brackets refer to the result obtained from the incoherent sum of the magnetic and electric amplitude.

82 MeV/u	$\mu_f = +1/2$	$\mu_f = -1/2$	$\mu_f = +3/2$	$\mu_f = -3/2$	Σ
$2s_{1/2}$	0.958	0.006			0.964
$2p_{1/2}$	0.384	0.452			0.836
$2p_{3/2}$	0.747	0.110	0.449	0.004	1.31
119 MeV/u	$\mu_f = +1/2$	$\mu_f = -1/2$	$\mu_f = +3/2$	$\mu_f = -3/2$	Σ
$2s_{1/2}$	0.825	0.006			0.831
	(1.010)	(0.000)			(1.010)
$2p_{1/2}$	0.356	0.549			0.905
	(0.680)	(0.449)			(1.129)
$2p_{3/2}$	0.729	0.137	0.561	0.005	1.432
	(1.173)	(0.180)	(0.540)	(0.0)	(1.893)
	[1.224]	[0.183]	[0.540]	[0.005]	[1.952]

B. He-like ions

Compared to the H-like species, the theoretical description of the excitation process for He-like systems is complicated by the correlated wave functions, which are needed for a complete description of the bound electron states. For high- Z ions, the electron-electron interaction is weak compared to the electron-nucleus interaction. Here, the most important relativistic effects are taken into account by using Dirac H-like wave functions. The description of high- Z He-like ions as a system of two independent electrons should therefore be an appropriate approach as long as the proper angular-momentum coupling scheme for the excited electron states is used (see Fig. 1). Note that this assumption has already been proven to provide a reasonable description of the K -shell excitation process even for an intermediate He-like Z system such as Fe^{24+} and Kr^{34+} [8–10].

In order to adopt the calculations performed for H-like Bi to the He-like system, the $[1s_{1/2}, 2s_{1/2}]_{J=0,1}$, $[1s_{1/2}, 2p_{1/2}]_{J=0,1}$, $[1s_{1/2}, 2p_{3/2}]_{J=1,2}$ levels are considered as hydrogenlike $2s_{1/2}$, $2p_{1/2}$, $2p_{3/2}$ states, respectively. The resulting population cross sections for the individual L -subshell levels are multiplied by a factor of two in order to account for the presence of two K -shell electrons in the initial state. For completeness, we add that the excitation cross sections in the He-like system are not corrected for their slightly different binding energies with respect to the H-like species. By applying the $1/(E_f - E_i)^2$ scaling law, valid for excitation and ionization, and by using exact binding energies for the levels in the H- and He-like ions, these corrections can be estimated to be less than 4% for excitation into all L -subshell levels.

III. EXPERIMENTAL ARRANGEMENT

The experiment was conducted at the fragment separator (FRS) at the heavy ion accelerator facility at GSI-Darmstadt. For the experiment, bismuth ions with a charge state of 67+ were accelerated in the heavy-ion synchrotron SIS to final energies of 82 and 119 MeV/u, respectively. The beam was extracted from SIS towards the FRS by using a slow extraction mode (spill length of about 2 s and repetition rate of 1 spill per 6 s). Using Al stripper foils, installed at the entrance of the FRS, the projectile charge state of 81+ (He-like) at 82 MeV/u and of 82+ (H-like) at 82 MeV/u and 119 MeV/u were produced. These charge states were selected and focused on thin solid targets using the first two stages of the FRS (carbon, aluminum, and nickel foils with thicknesses of 550, 490, and 130 $\mu\text{g}/\text{cm}^2$, respectively). After passing through the target, the beam was magnetically analyzed and directed onto three plastic scintillator counters. These allowed us to register separately ions with primary charge state (middle one) and those having captured or lost one electron. For the detection of characteristic projectile x rays, the target area was viewed by two fivefold, 5-mm-thick, planar germanium detectors mounted perpendicularly to the beam direction. One detector was mounted close to the target, with a solid angle of about 1% of 4π . For the other detector, the beam-to-detector distance was chosen such that the observed Doppler broadening was smaller than the *L*-shell fine-structure splitting. Both detectors were separated from the high-vacuum system of the beam line by 50- μm -thick stainless steel windows. The signal rise time of these detectors, about 50 ns, determined the time resolution for the x-ray-particle coincidences. The coincidence technique was applied in order to distinguish x-ray events associated with projectiles leaving the target with the primary charge state and those having captured one electron. This allowed us to separate projectile x-ray emission produced by Coulomb excitation from that induced by electron capture into the projectile. For a detailed description of the setup used we refer to Refs. [2,15].

IV. X-RAY SPECTRA AND DATA ANALYSIS

Figure 4 shows sample x-ray spectra recorded for initially He-like Bi^{81+} ions colliding with carbon atoms at a beam energy of 82 MeV/u. The two spectra were taken using the central segment of the distant Ge(i) detector in coincidence with ions of the primary charge state of 81+ (without charge exchange) [Fig. 4(a)] and with ions having captured one electron [Fig. 4(b)]. Both spectra are corrected for the Doppler shift and for the x-ray detection efficiency, whereas the spectra are not corrected for photon absorption in the stainless steel x-ray windows. In addition, random coincidences have been subtracted. The spectrum measured in coincidence with the primary charge state [no projectile charge exchange, Fig. 4(a)] is dominated by continuous x-ray radiation appearing at low energies, which is attributed to primary bremsstrahlung. In this process, a target electron is transferred into the projectile continuum with simultaneous emission of a photon. The intensity of the x-ray continuum decreases strongly with increasing photon energy and the high-energy end point of this continuum is located approximately at energies corresponding to the kinetic energy, E_{KIN} , of an im-

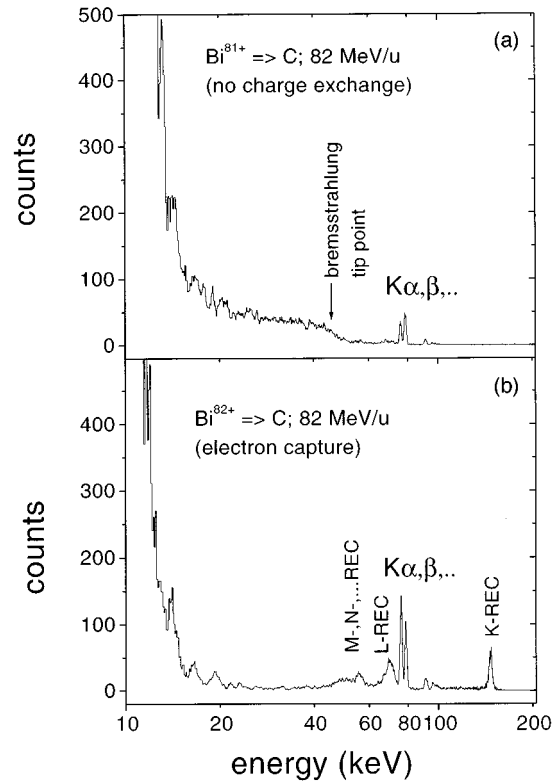


FIG. 4. Sample x-ray spectra recorded for initially He-like Bi^{81+} ions colliding with carbon atoms. The two spectra were taken by the central segment of the distant Ge(i) detector in coincidence with the primary charge state of 81+ (a) and with the ions having captured one electron (b). Both spectra are corrected for the Doppler shift and for the x-ray detection efficiency whereas the spectra are not corrected for photon absorption in the stainless steel x-ray windows.

compact electron moving with the primary projectile velocity. For 82 MeV/u it corresponds to about 45 keV. Note that due to photon absorption in the x-ray window used, the spectral shape of the bremsstrahlung appears to be deformed and, in particular, the bremsstrahlung intensity is strongly reduced at energies below 50 keV. Above the threshold of the bremsstrahlung, the x-ray spectrum [Fig. 4(a)] is governed by the ground-state projectile transitions, i.e., by $K\alpha$, $K\beta$, $K\gamma$, etc. radiation. Since at such low projectile energies these transitions are energetically well separated from the bremsstrahlung continuum, almost no background is visible above 50 keV.

In contrast to the spectrum shown in Fig. 4(a), the x-ray spectrum associated with capture of one target electron into the H-like projectiles is strongly influenced by radiative electron capture into the vacant $1s$ projectile shell, a process that can be considered as the time reversed photoionization [21,22]. The most prominent line appears at about 140 keV and is attributed to the transition of quasi-free-target electrons into the projectile *K* shell (*K* REC). In the following we concentrate on the x-ray energy regime relevant for the ground state transitions in H- and He-like bismuth. In Fig. 5, x-ray spectra are given that were recorded for 82 MeV/u $\text{Bi}^{82+} \rightarrow \text{C}$ ($\text{Bi}^{81+} \rightarrow \text{C}$) collisions by the central segment of the distant detector [Fig. 5(a): excitation of H-like Bi^{82+} ; Fig. 5(b): excitation of He-like Bi^{81+} ; Fig. 5(c): electron capture from the target atom into H-like Bi^{82+} forming ex-

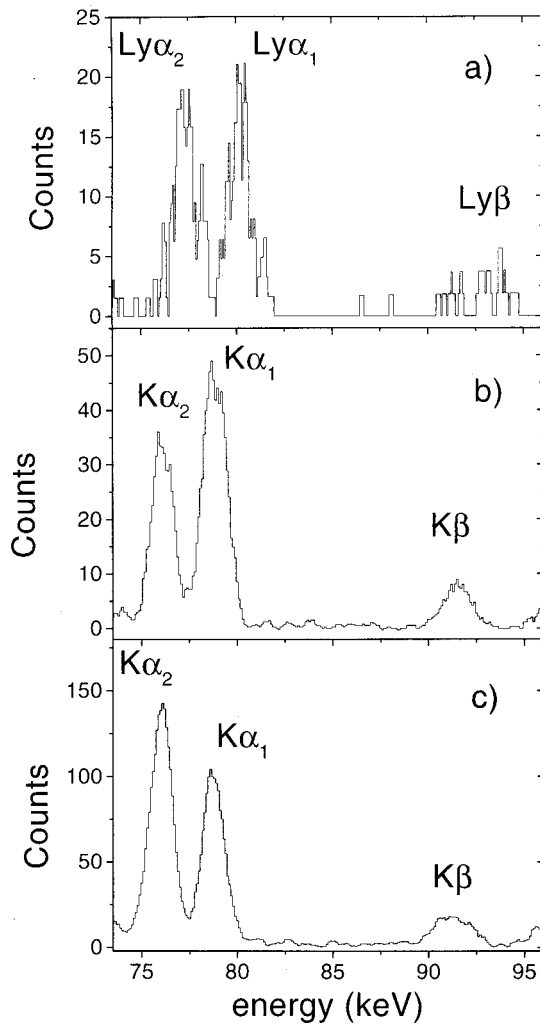


FIG. 5. Lyman and K x-ray energy regime measured by the central segment of the distant detector for excitation of H-like Bi^{82+} (a), for excitation of He-like Bi^{81+} (b), and for capture into H-like Bi^{82+} leading to ground-state transitions in He-like Bi^{81+} (c). All the spectra were recorded for the carbon target at a beam energy of 82 MeV/u.

cited levels in He-like Bi^{81+}). The most striking feature of the spectra is the observed difference in the relative intensities of the $\text{Ly}\alpha$ ($K\alpha$) doublet. These intensities depend on the charge state of the ion used as well as on the population mechanism of the excited L -shell levels. The latter follows directly from a comparison of the Figs. 4(b) and 4(c). In both cases the excited L -subshell levels in He-like Bi are formed, in the first case by ground-state excitation [Fig. 5(b)] and in the second case by electron capture [Fig. 5(c)]. The observed difference in the $K\alpha$ line intensity pattern illustrates convincingly that the population characteristics of excited states are completely different for the two processes. Note that, the intensity pattern observed in Fig. 5(c) is typical for electron capture reactions taking place in fast collisions of high- Z projectiles and low- Z targets [23]. In the case of excitation in H-like Bi^{82+} the two $\text{Ly}\alpha$ components exhibit an almost equal intensity and the $\text{Ly}\alpha$ lines are slightly shifted to higher x-ray energies with respect to the $K\alpha$ transitions in He-like Bi [compare Fig. 5(a) and Fig. 5(b)].

For data evaluation, the spectra of all segments of both

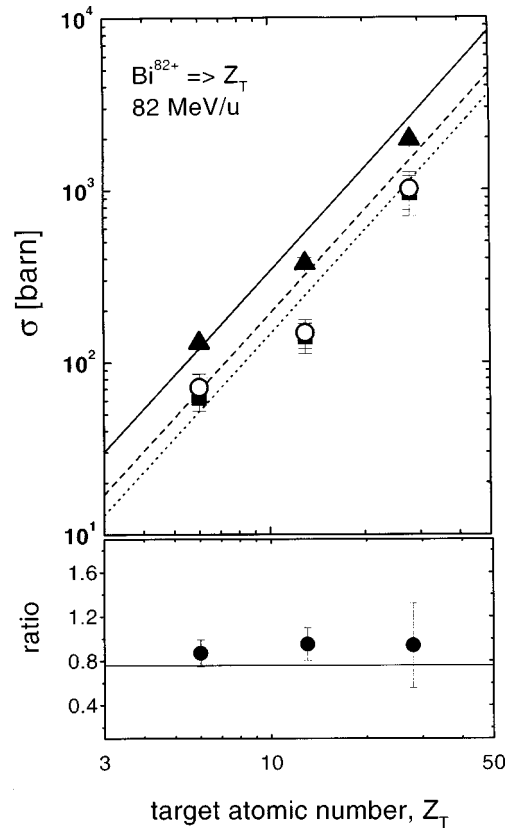


FIG. 6. L -subshell resolved K -shell excitation cross sections (upper part) obtained for H-like bismuth ions at 82 MeV/u in collisions with the C, Al, and Ni [$\text{Ly}\alpha_1$ (open points), $\text{Ly}\alpha_2$ (solid squares), total $\text{Ly}\alpha$ (solid triangles)]. The data are compared with the results of the relativistic cross-section calculations (dotted line: $\text{Ly}\alpha_1$; dashed line: $\text{Ly}\alpha_2$; solid line: total $\text{Ly}\alpha$). In the bottom part the theoretical (full lines) and the experimental (full points) $\text{Ly}\alpha_1$ to $\text{Ly}\alpha_2$ intensity ratios are compared. The error bars refer to the statistical uncertainty only.

detectors were used. In the first step the true and random x-ray spectra for each individual segment were obtained by setting appropriate time windows on the time spectra associated with x-ray-particle coincidences. After subtraction of the random spectra from the true coincident x-ray spectra the results were corrected for the x-ray detection efficiency. Subsequently, the $\text{Ly}\alpha$ and $K\alpha$ transitions observed by all the segments were fitted by Gaussian distributions. In addition, a linear background was considered within the applied least-square fitting procedure. Finally, the line intensities were normalized to the total charge-exchange rate and corrected for the electronic dead time. Considering the uncertainties due to the target thickness, photon and particle detection efficiencies, and the stability of the beam geometry we estimate that the overall systematic error amounts to 10% (for a detailed discussion we refer to [2,15,24]).

V. RESULTS AND DISCUSSION

A. $K \rightarrow L$ -shell excitation cross sections for H-like projectiles

In the upper parts of Fig. 6 and Fig. 7 the L subshell resolved cross sections for K x-ray emission associated with projectile excitation are displayed. They were measured for

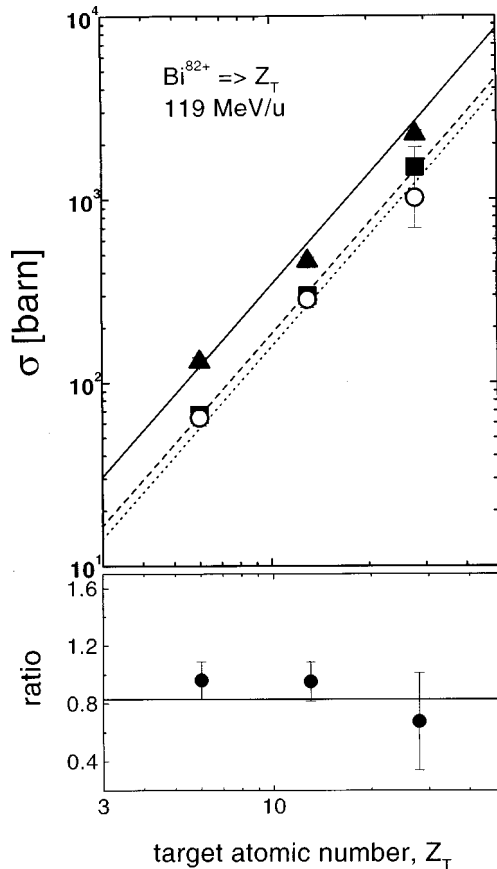


FIG. 7. L -subshell resolved K -shell excitation cross sections (upper part) obtained for H-like bismuth ions at 119 MeV/u in collisions with the C, Al, and Ni [$\text{Ly-}\alpha_1$ (open points), $\text{Ly-}\alpha_2$ (solid squares), total $\text{Ly-}\alpha$ (solid triangles)]. The data are compared with the results of the relativistic cross-section calculations (dotted line: $\text{Ly-}\alpha_1$; dashed line: $\text{Ly-}\alpha_2$; solid line: total $\text{Ly-}\alpha$). In the bottom part the theoretical (full lines) and the experimental (full points) $\text{Ly-}\alpha_1$ to $\text{Ly-}\alpha_2$ intensity ratios are compared. The error bars refer to the statistical uncertainty only.

H-like bismuth ions in collisions with C, Al, and Ni targets at 82 MeV/u (Fig. 6) and at 119 MeV/u (Fig. 7). In the figures the cross-section data for $\text{Ly-}\alpha_1$ (open points) and for $\text{Ly-}\alpha_2$ (solid squares) are given separately versus the nuclear charge of the target. Also the total $\text{Ly-}\alpha$ production cross sections are depicted (solid triangles). These were deduced independently by the second x-ray detector mounted close to the beam line (see Sec. III). The experimental data are compared with the theoretical calculations (see Sec. II and also theoretical cross section values given in the table) of the $\text{Ly-}\alpha_1$ (dotted line), the $\text{Ly-}\alpha_2$ (dashed line), and the total $\text{Ly-}\alpha$ production cross sections following K -shell excitation. With respect to the $2p_{3/2}$ state we note that an alignment of this level is predicted by the calculations. It leads to an anisotropic angular distribution of the $\text{Ly-}\alpha_1$ radiation, which results in a 2% larger differential cross section compared to an isotropic emission pattern at 90° observation angle. For completeness, we corrected the experimental data for this effect.

For the theoretical $\text{Ly-}\alpha_1$ cross section, excitation to the $2p_{3/2}$ level was considered whereas the cross sections for the production of $\text{Ly-}\alpha_2$ transitions were calculated by taking into account excitation to the $2s_{1/2}$ and to the $2p_{1/2}$ state.

Also the cascade contributions due to excitation into the M shell were taken into account by calculating the individual excitation cross sections into the M subshells and by using the corresponding $M \rightarrow L$ transition rates obtained from the GRASP code [25]. From the latter it turned out that at both energies and for all excited levels, population by cascade feeding contributes about 9% to the total population cross section. Excitation via target electron impact (so-called anti-screening) is not considered since the threshold for this process is close to 145 MeV/u, i.e. far above the beam energies used in the experiment.

From the comparison between experimental data and the theoretical predictions given in Fig. 6 and Fig. 7, an overall good agreement can be seen. In particular, the data confirm the validity of the Z^2 scaling law, which is strictly valid within first order perturbation theory. Whereas for 119 MeV/u an almost perfect agreement between experiment and theory is found, only a fair agreement is seen for 82 MeV/u, where the experimental data deviate by as much as about 50% (Al target) from the theoretical predictions. Here, it is important to note that the error bars given in the figure depict the statistical uncertainties only. For the case of the H-like projectiles at 82 MeV/u, however, an additional source of error must be taken into account, i.e., the uncertainty introduced by the subtraction of a considerable amount of random coincidences. These are caused mainly by the large electron capture cross sections from the target into the projectile, which yield a $K\alpha$ intensity that is almost two orders of magnitude stronger than for Coulomb excitation. We estimate the size of this uncertainty to be of the order of 20% which is expected to affect the absolute cross-section values. The latter can be seen by comparison of the theoretical (full lines) and experimental (full points) $\text{Ly-}\alpha_1$ to $\text{Ly-}\alpha_2$ intensity ratios presented in the bottom parts of Fig. 6 and Fig. 7. Here, for both energies, agreement was found that verified that the measured relative subshell cross sections are almost unaffected by systematic uncertainties. In addition, these ratios confirm the calculated relative cross sections for excitation into the $j=1/2$ sublevels with respect to excitation into the $2p_{3/2}$ level. In contrast to a nonrelativistic approach, the predicted $2p_{3/2}/2p_{1/2}$ cross-section ratio (compare values given in the table) does not reflect the statistical weight of the levels.

In the following, we concentrate on the role of the magnetic interaction for the excitation or ionization process in relativistic ion-atom collisions. As discussed in detail in Sec. II, the consideration of the magnetic parts of the interaction leads to a strong reduction of the absolute cross section values pointing to a destructive interference between the amplitudes for the electric and magnetic part of the interaction. In fact, these theoretical findings seem to be confirmed by the experimental data. Since the measured $\text{Ly-}\alpha_1$ production cross section is caused by excitation to only one level ($2p_{3/2}$), we compare in Fig. 8 the reduced cross-section values (σ/Z_T^2) measured at 119 MeV/u with theoretical predictions obtained with (solid line) and without (dashed line) the magnetic part of the Liénard-Wiechert interaction. As can be seen from the figure, the experimental data favor the result of the complete calculation. This shows that the inclusion of the

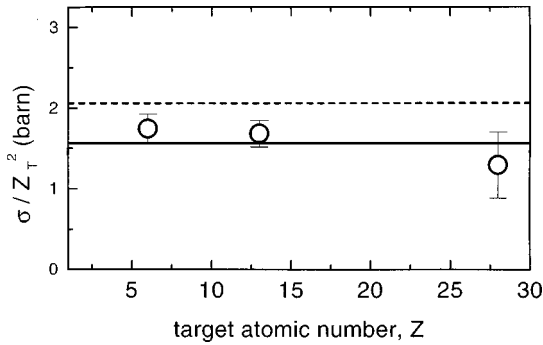


FIG. 8. Reduced Ly- α_1 cross-section values (σ/Z_T^2) measured at 119 MeV/u in comparison with the theoretical predictions obtained with (full line) and without (dashed line) the magnetic part of the Liénard-Wiechert interaction.

full Liénard-Wiechert interaction leads to a strong cross-section reduction. This is in contrast to a commonly used assumption that the magnetic part of the interaction must lead to a cross-section enhancement [14].

B. $K \rightarrow L$ -shell excitation cross-sections for He-like projectiles

In the upper part of Fig. 9, the L -subshell differential K -shell excitation cross sections that were obtained for He-like bismuth ions at an energy of 82 MeV/u in collisions with C, Al, and Ni targets are displayed. The production cross sections for $K\alpha_2$ (solid squares) and for $K\alpha_1$ (open circles) radiation, measured with the distant x-ray detector, are given separately versus the nuclear charge of the target. In addition, also the total $K\alpha$ production cross sections are given in the figure (up-triangles) as measured by the detector mounted close to the beam line. Again, the data sets for both detectors are consistent within their statistical errors. The lines in the figure (dotted line: $K\alpha_2$ production cross section; dashed line: $K\alpha_1$ production cross section, full line: total $K\alpha$ production cross section) refer to the results of the relativistic calculations; in the bottom part the theoretical (solid line) and experimental (full points) $K\alpha_1$ to $K\alpha_2$ intensity ratios are compared. In addition, the $K\alpha_1$ to $K\alpha_2$ intensity ratio obtained from the $^3P_1/^1P_1$ mixing coefficient, derived from the GRASP code, is depicted by the dashed line.

For this purpose, the excitation cross sections into the M -shell levels were computed and the transition rates obtained from the GRASP code [25] were used. Similar to the H-like system, the population of the excited L levels via cascades contributes by about 9% to the total cross section. We have to stress that the data for the He-like ions are much more precise than the data obtained for H-like systems at the same beam energy of 82 MeV/u. Due to the blocked K shell, electron capture cannot lead to $K\alpha$ emission, thus improving significantly the accuracy of the measurement.

We have to stress the very good agreement between our experimental results and the calculations. In particular, this agreement confirms our treatment of the excitation process in high- Z He-like ions where the $K\alpha_2$ and $K\alpha_1$ intensities are basically determined by the excitation cross sections for the $2p_{1/2}$ and the $2p_{3/2}$ levels, respectively in the H-like species. This is shown in even more detail in the bottom part of Fig. 9, where the measured $K\alpha_1$ to $K\alpha_2$ intensity ratio is plotted for different Z_T . In the figure, the theoretical cross-section ratio is given by the solid line. We have also calculated the $K\alpha_1$ to $K\alpha_2$ intensity ratio by using the $^3P_1/^1P_1$ mixing

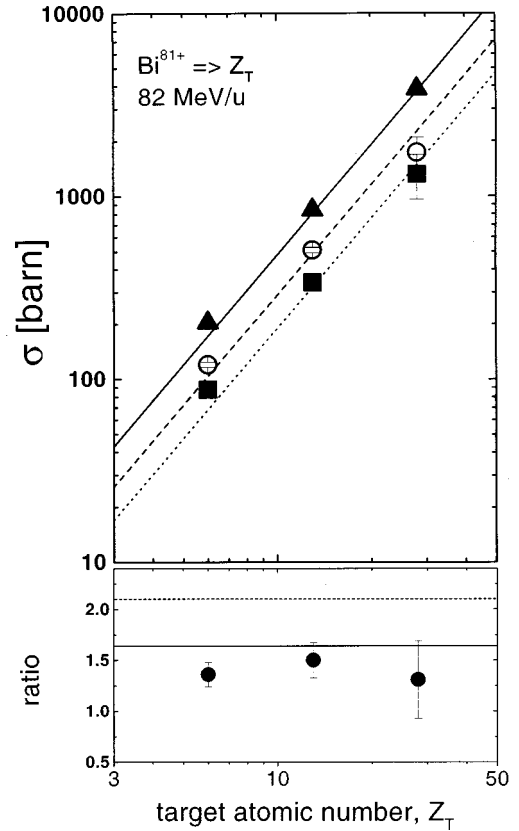


FIG. 9. L -subshell resolved K -shell excitation cross sections obtained for He-like bismuth ions at 82 MeV/u in collisions with the C, Al, and Ni. The cross-section data for $K\alpha_1$ (open points), $K\alpha_2$ (solid squares), and the total $K\alpha$ cross sections (solid triangles) are compared with the results of the relativistic calculations; dotted line: $K\alpha_1$ production cross section, dashed line: $K\alpha_2$ production cross section, full line: total $K\alpha$ production cross section. In the bottom part the theoretical (solid line) and experimental (full points) $K\alpha_1$ to $K\alpha_2$ intensity ratios are compared. In addition, the $K\alpha_1$ to $K\alpha_2$ intensity ratio obtained from the $^3P_1/^1P_1$ mixing coefficient, derived from the GRASP code, is depicted by the dashed line.

calculation. For this purpose, the excitation cross sections into the M -shell levels were computed and the transition rates obtained from the GRASP code [25] were used. Similar to the H-like system, the population of the excited L levels via cascades contributes by about 9% to the total cross section. We have to stress that the data for the He-like ions are much more precise than the data obtained for H-like systems at the same beam energy of 82 MeV/u. Due to the blocked K shell, electron capture cannot lead to $K\alpha$ emission, thus improving significantly the accuracy of the measurement.

We have to stress the very good agreement between our experimental results and the calculations. In particular, this agreement confirms our treatment of the excitation process in high- Z He-like ions where the $K\alpha_2$ and $K\alpha_1$ intensities are basically determined by the excitation cross sections for the $2p_{1/2}$ and the $2p_{3/2}$ levels, respectively in the H-like species. This is shown in even more detail in the bottom part of Fig. 9, where the measured $K\alpha_1$ to $K\alpha_2$ intensity ratio is plotted for different Z_T . In the figure, the theoretical cross-section ratio is given by the solid line. We have also calculated the $K\alpha_1$ to $K\alpha_2$ intensity ratio by using the $^3P_1/^1P_1$ mixing

coefficient derived from the GRASP code, a method commonly applied for the intermediate- Z range [8]. From the latter, a $K\alpha_1$ to $K\alpha_2$ intensity ratio of 2.1 is obtained, which fails to describe our experimental data.

VI. SUMMARY

Projectile K -shell excitation has been studied both experimentally and theoretically in encounters of heavy one- and two-electron bismuth ions ($Z=83$) with light solid targets. By applying an x-ray-particle coincidence technique, excitation of the K -shell electrons into the L -shell sublevels was observed via registration of Ly- α and $K\alpha$ photons from H- and He-like Bi ions associated with the primary charge state, i.e., separated from the projectile photon emission induced by electron-capture processes. Since such subshell-differential experiments are only sensitive to a very limited number of excitation modes (in the nonrelativistic limit only monopole and dipole excitation contributes), the data obtained provide a more detailed test of atomic collision theory than ionization cross-section data. The experimental results were compared with theoretical predictions based on a fully relativistic first-order perturbation approach, which considers the complete Liénard-Wiechert interaction. With respect to the absolute cross sections for excitation into the individual L -subshell levels, an overall good agreement between experiment and theory is found. This agreement confirms the theoretical result that even at our low- β values magnetic effects are already of considerable relevance. In particular, they show that the magnetic part of the Liénard-Wiechert potential leads to a strong reduction of the absolute cross-section values. This points to an interference between the amplitudes for the magnetic and electric part of the interaction, i.e., to a breakdown of a commonly used quasirelativistic approach [26,27] where the amplitudes of the Coulomb part and of the magnetic part of the interaction are added up incoherently. Until now, such interferences were not observed for high- Z ions. Previously, only total cross-section data for projectile ionization were available and these are in general agreement with the predictions of the quasirelativistic treatment.

For the case of He-like Bi, our experimental findings underline the basic assumption that only excitation to the p states of the L shell is observed in the experiment. In particular, the data are found to be in good agreement with the assumption that in the case of Coulomb excitation, the high- Z He-like ions behave like one-electron systems, i.e., the $[1s_{1/2}, 2p_{1/2}]_{J=1}$ and the $[1s_{1/2}, 2p_{3/2}]_{J=1}$ states can be treated as the $2p_{1/2}$ and the $2p_{3/2}$ states, respectively. In order to clarify this point and to investigate the relevance of electron-correlation effects for the process of K -shell excitation or ionization, complete relativistic calculations with correlated two-electron wave functions are needed. Such calculations would also clarify the relative population of the states with different total angular momentum J ($[1s_{1/2}, 2p_{1/2}]_{J=0,1}$, $[1s_{1/2}, 2p_{3/2}]_{J=1,2}$). At this time, these calculations are not available.

One of the limitations of the present experiment is that, because of the dense targets used, we cannot completely exclude double-step processes such as $\Delta n=0$ excitation or ionization followed by electron capture [2]. Therefore, for future investigations with H- and He-like high- Z systems, the gas-jet target of the storage ring ESR with typical areal densities of 10^{+12} particles/cm² appears to be most appropriate. Here double step processes are nearly excluded. Also, in such experiments it would be interesting to measure the angular distribution of the decay radiation in order to determine the alignment that provides more detailed information about the excitation process than total cross-section measurements.

ACKNOWLEDGMENTS

The authors would like to thank J. Eichler for his helpful comments on the manuscript. The work of two of us (Z. S. and A. W.) was supported in part by the State Committee for Scientific Research (Poland) under research Grant No. 2P03B10910 and by GSI in Darmstadt. R. W. D. was supported by GSI and the U.S. DOE Office of Basic Energy Sciences. P. R. was supported by GSI and by the State Committee for Scientific Research (Poland) under research Grant No. 2P30211907.

-
- [1] For a summary of relativistic atomic collisions, see, e.g., J. Eichler and W.E. Meyerhof, *Relativistic Atomic Collisions* (Academic Press, San Diego, 1995).
 - [2] Th. Stöhlker, C. Kozhuharov, P.H. Mokler, A. Warczak, F. Bosch, H. Geissel, R. Moshhammer, C. Scheidenberger, J. Eichler, A. Ichihara, T. Shirai, Z. Stachura, and P. Rymuza, *Phys. Rev. A* **51**, 2098 (1995).
 - [3] D. Detleffsen, M. Anton, A. Werner, and K.H. Schartner, *J. Phys. B* **38**, 4195 (1994).
 - [4] K. Reymann, K.H. Schartner, B. Sommer, and E. Träbert, *Phys. Rev. A* **27**, 2290 (1988).
 - [5] M. Anton, D. Detleffsen, K.H. Schartner, and A. Werner, *J. Phys. B* **26**, 2005 (1993).
 - [6] N. Stolterfoht, *J. Electron Spectrosc. Relat. Phenom.* **67**, 309 (1993).
 - [7] N. Stolterfoht, A. Mattis, D. Schneider, G. Schiwietz, B. Skogvall, B. Sulik, and S. Ricz, *Phys. Rev. A* **51**, 350 (1995).
 - [8] K. Wohrer, A. Chetioui, J.P. Rozet, A. Jolly, F. Fernandez, C. Stephan, B. Brendle, and R. Gayet, *J. Phys. B* **19**, 1997 (1986).
 - [9] L. Adoui, D. Vernhet, K. Wohrer, J. Plante, A. Chetioui, J.P. Rozet, I. Despiney, C. Stephan, A. Touati, J.M. Ramillion, A. Cassimi, J.P. Grandin, and M. Cornille, *Nucl. Instrum. Methods Phys. Res. B* **98**, 312 (1995).
 - [10] D. Vernhet, J.P. Rozet, K. Wohrer, L. Adoui, C. Stephan, A. Cassimi, and J.M. Ramillion, *Nucl. Instrum. Methods Phys. Res. B* **107**, 71 (1996).
 - [11] B. Brendle, R. Gayet, J.P. Rozet, and K. Wohrer, *Phys. Rev. Lett.* **54**, 2007 (1985).
 - [12] G. Mehler, G. Soff, K. Rumrich, and W. Greiner, *Z. Phys. D* **13**, 193 (1989).
 - [13] K. Rumrich, G. Soff, and W. Greiner, *Phys. Rev. A* **47**, 215 (1993).

- [14] R. Anholt and U. Becker, *Phys. Rev. A* **36**, 4628 (1987).
- [15] P. Rymuza, Th. Stöhlker, C.L. Cocke, H. Geissel, C. Kozhuharov, P.H. Mokler, R. Moshhammer, F. Nickel, C. Scheidenberger, Z. Stachura, J. Ullrich, and A. Warczak, *J. Phys. B* **26**, L169 (1993).
- [16] Th. Stöhlker, *Phys. Lett. A* (to be published).
- [17] P.H. Mokler, Th. Stöhlker, C. Kozhuharov, R. Moshhammer, P. Rymuza, F. Bosch, and T. Kandler, *Phys. Scr.* **T51**, 28 (1994).
- [18] S. Cheng, H.G. Berry, R.W. Dunford, D.S. Gemmell, E.P. Kanter, C. Kurtz, K.E. Rehm, and B.J. Zabransky, *Phys. Rev. A* **50**, 2197 (1994).
- [19] M.E. Rose, *Relativistic Electron Theory* (Wiley, New York, 1961).
- [20] N. Toshima and J. Eichler, *Phys. Rev. A* **38**, 2305 (1988).
- [21] A. Ichihara, T. Shirai, and J. Eichler, *Phys. Rev. A* **54**, 4955 (1996).
- [22] Th. Stöhlker, Ph. Mokler, C. Kozhuharov, and A. Warczak, *Comments At. Mol. Phys.* **33**, 271 (1997).
- [23] Th. Stöhlker, P.H. Mokler, K. Beckert, F. Bosch, H. Eickhoff, B. Franzke, G. Geissel, M. Jung, T. Kandler, O. Klepper, C. Kozhuharov, R. Moshhammer, F. Nickel, F. Nolden, H. Reich, P. Rymuza, C. Scheidenberger, P. Spädtke, Z. Stachura, M. Steck, and A. Warczak, *Nucl. Instrum. Methods Phys. Res. B* **87**, 64 (1994).
- [24] Th. Stöhlker, P.H. Mokler, H. Geissel, R. Moshhammer, P. Rymuza, E.M. Bernstein, C.L. Cocke, C. Kozhuharov, G. Münzenberg, F. Nickel, C. Scheidenberger, Z. Stachura, J. Ullrich, and A. Warczak, *Phys. Lett. A* **168**, 285 (1992).
- [25] K. Dyllal *et al.*, *Comput. Phys. Commun.* **55**, 425 (1989).
- [26] R. Anholt, *Phys. Rev. A* **19**, 1004 (1979).
- [27] R. Anholt and H. Gould, in *Advances in Atomic and Molecular Physics* (Academic, New York, 1986), Vol. 22, p. 315.